



# Silver nanowires with different concentration for Q-switched fiber lasers

MENGLI LIU,<sup>1</sup> WENJUN LIU,<sup>1,2,\*</sup>  HUANRAN HOU,<sup>1</sup> YUYI OUYANG,<sup>1</sup> MING LEI,<sup>1</sup> AND ZHIYI WEI<sup>2</sup> 

<sup>1</sup>State Key Laboratory of Information Photonics and Optical Communications, School of Science, P. O. Box 122, Beijing University of Posts and Telecommunications, Beijing 100876, China

<sup>2</sup>Beijing National Laboratory for Condensed Matter Physics, Institute of Physics, Chinese Academy of Sciences, Beijing 100190, China

\*jungliu@bupt.edu.cn

**Abstract:** Silver nanowire (AgNW) has become preferred due to its excellent performance in terms of biocompatibility, transparency, heat transfer and conductivity, and thus has been widely used in catalysts, microelectronic devices, sensors, solar cells, etc. Although some related properties of which have aroused great interest, the nonlinear optical properties of AgNW in laser have not been reported so far. In this paper, the nonlinear optical properties of AgNW are explored in Q-switched fiber laser. Additionally, the effects of three different AgNWs on the performance of corresponding Q-switched lasers are investigated. Results show that the concentration, saturation intensity, insertion loss and modulation depth of AgNW have great influence on the performance of lasers. Moreover, compared with similar SA-based lasers, the AgNW-based laser implemented has bright application prospects in the generation of ultrashort pulses.

© 2019 Optical Society of America under the terms of the [OSA Open Access Publishing Agreement](#)

## 1. Introduction

Nanomaterials refer to materials with structure unit size of the nanometer scale. On the one hand, nanomaterials can produce strong interactions due to their small coherence lengths, thus exhibiting completely different properties from bulk materials. On the other hand, their nanometer size makes them have a special performance of large surface effect. This special structure prompts nanomaterials to show unique nature, including dielectric confinement effects, macroscopic quantum tunneling effects, quantum size effects, interface effects and small size effects [1]. Among them, two-dimensional (2D) materials have aroused an upsurge of research. Since the first 2D material, graphene, was introduced in 2004 [2–7], about 700 2D materials have been experimentally or theoretically certified to exist [8–10]. Some of these materials, such as black phosphorus, topological insulator, and transition metal dichalcogenides (TMD), have been used in applications such as photovoltaics, semiconductors, electrodes, optical devices and sensing [11–20].

Meanwhile, the tremendous progress of other nanomaterials in theoretical research and commercial applications should not be underestimated [21–34]. In the catalysis, the silver nanomaterials with uniform size and high aspect ratio have a large reaction area and strong oxygen reduction ability, which improve the total electric efficiency of the lithium oxide battery by 83.4% [35]. In addition, AgNWs have become the focus of electrode materials because of their excellent performance in terms of transparency and conductivity, the flexible transparent conductive films based on which can be widely used in liquid crystal display and wearable electronic devices [36,37]. Meanwhile, it was reported that the AgNW electrode prepared by Lee et al. has good electrical conductivity and transmittance of 87.6%, which can be used to replace ITO materials in organic light-emitting diodes and solar cells [38]. Besides, sensor based on

AgNW not only has high sensitivity and ultra-fast response time, but also exhibits great stability in a given environment [39,40].

In recent years, the optical property of AgNW is becoming a cause for concern. By using Z-scan technology, the third-order nonlinear polarizability of AgNW is investigated [41], which is found comparable to TMD material [42]. Besides, it was reported that the lifetime of plasmon in the AgNW is  $150 \pm 7$  fs [43], which is smaller than graphene [44]. Therefore, AgNW has great advantages in the realization of ultrafast fiber lasers.

In this paper, the nonlinear optical properties of proposed AgNW SAs are investigated experimentally with the ideal platform of Q-switched fiber laser (QSFL). Meanwhile, the effects of three different AgNW SAs on QSFLs are explored through comparative experiments. The results show that both the concentration, saturation intensity, insertion loss and modulation depth of AgNW have a influence on the performance of lasers. Furthermore, the pulse duration of 536 ns and average output power of 34.7 mW are achieved based on the AgNW SA with concentration of 1 mg/mL, which is competitive with similar lasers. Our research indicates the great potential of AgNW in the generation of ultrashort pulse, and paves the way for the subsequent engineering design of related optical devices.

## 2. Preparation and characterization of AgNW SA

The AgNWs used in the experiment were prepared by the classical hydrothermal method, which is conducive to the acquisition of samples with high purity, good dispersion, uniformity and crystalline form. Three ingredients, such as copper chloride dihydrate ( $\text{CuCl}_2 \cdot 2\text{H}_2\text{O}$ ), polyvinylpyrrolidone (PVP), and silver nitrate ( $\text{AgNO}_3$ ) are all put into the container and stirred sufficiently to achieve uniform mixing. After 10 minutes of stirring, the formed precursor solution is heated at 130 °C temperatures for up to 3 hours. Then, AgNWs with high purity are obtained. Prepared AgNWs are subsequently diffused into ethanol (EtOH) for use. By diffusing unequal amounts of AgNW into EtOH, three samples with different concentrations such as 2 mg/mL, 1 mg/mL and 0.5 mg/mL are obtained. The prepared solutions were spin-coated on the end surfaces of fiber ferrules as SAs at a speed of 1500 rpm.

The X-ray diffraction (XRD) pattern of prepared AgNW is shown in Fig. 1(a). There are three distinct diffraction peaks including (111), (200) and (220), which can be indexed to the face-centered cubic structure of silver according to the reported data (JCPDS File No. 87-0718). X-ray photoelectron spectroscopy (XPS), as an important method for distinguishing material components and valence states of materials, is able to effectively help to identify the form of silver in the sample. As shown in Fig. 1(b), two peaks at 374.1 eV and 368.1 eV correspond to  $\text{Ag}3d_{3/2}$  and  $3d_{5/2}$ , which are reported as the typical values of  $\text{Ag}^0$  [45]. XPS demonstrates the inclusion of metallic silver in the product, further eliminating the presence of silver nitrate residues and silver oxides. The linear absorption of AgNW with different concentrations is shown in Fig. 1(c), which indicates that the absorptivity increases with the increase of concentration. Transmission electron microscope (TEM) is always used to investigate the microstructure and morphology of materials. As shown in Fig. 1(d), the different positions of the nanowires almost maintain a diameter of 50 nm, which indicates that the material is relatively uniform. The electron diffraction pattern in the illustration of Fig. 1(d) confirms that the AgNW tested had only one set of diffraction patterns, indicating that the material is a single crystal structure.

Scanning electron microscope (SEM) is considered to be an effective method to measure the surface topography of materials. The density variation of materials with different concentrations are clearly observed in Fig. 2(a) (sample1: 2 mg/mL), Fig. 2(b) (sample 2: 1 mg/mL) and Fig. 2(c) (sample 3: 0.5 mg/mL). The thicknesses of three materials are measured by atomic force microscopy (AFM) as shown in Fig. 2(d)–2(i). Although AgNWs are considered to be one-dimensional nanostructures, when the number is more than one, overlaps and cross junctions inevitably occur between the nanowires. Because the probability and the number of overlaps and

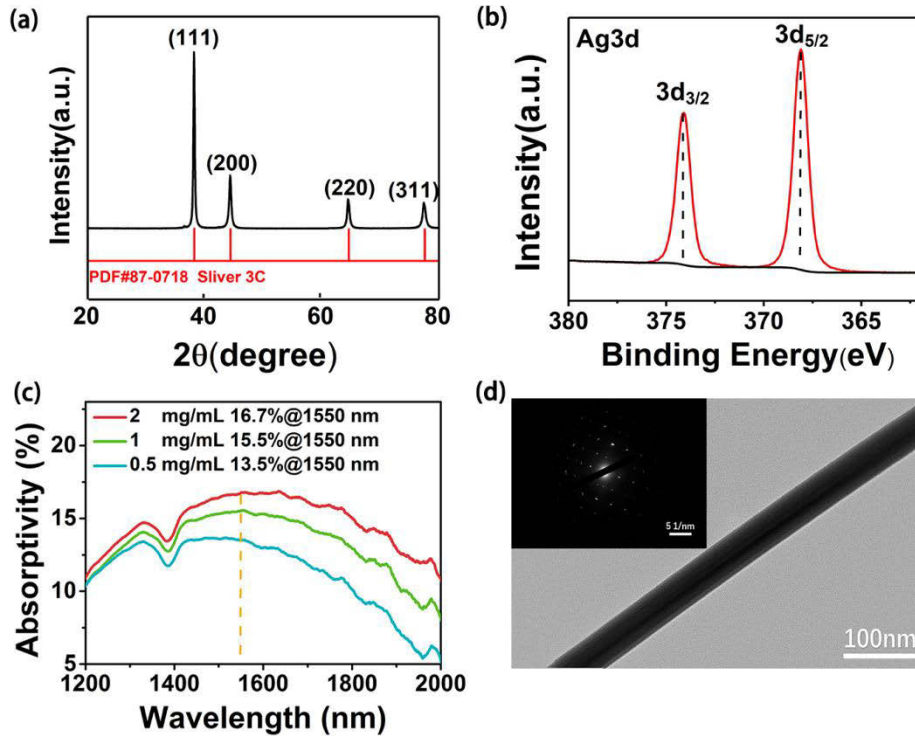


**Fig. 1.** (a) The XRD, (b) XPS, (c) linear optical absorption and (d) TEM of AgNW.

cross junctions appearing in sample 1 with a higher concentration are more as shown in Figs. 2(d) and 2(g), while those in sample 3 with lower concentration are less as shown in Fig. 2(f) and 2(i). Therefore, from the AFM in Fig. 2(d)–2(i), the greater the concentration, the larger the D-value in thickness. The nonlinear transmission properties of three AgNW SAs are investigated by a typical 2-arm transmission measurement. The center wavelength, pulse duration, repetition rate and average power of used mode-locked laser are 1553 nm, 600 fs, 120 MHz and 11.9 mW, respectively. The measurement results and fitting curves are shown in Fig. 2(j)–2(l). The absorption coefficient of saturated absorber decreases with the increase of incident light intensity, and it is “transparent” to laser when it reaches the saturation value. The saturable absorption mechanism is theoretically expressed as

$$\alpha(I) = \frac{\alpha_s}{1 + I/I_{sat}} + \alpha_{ns}.$$

By fitting, the modulation depth ( $\alpha_s$ ) of sample 1 is 46.19%, with saturation intensity ( $I_{sat}$ ) of 2.256 MW/cm<sup>2</sup> and non-saturable loss ( $\alpha_{ns}$ ) of 5.481%. Similarly, the  $\alpha_s$ ,  $I_{sat}$  and  $\alpha_{ns}$  of sample 2 and sample 3 are 26.23%, 6.819 MW/cm<sup>2</sup>, 4.243% and 13.79%, 10.36 MW/cm<sup>2</sup>, 9.424%, respectively.

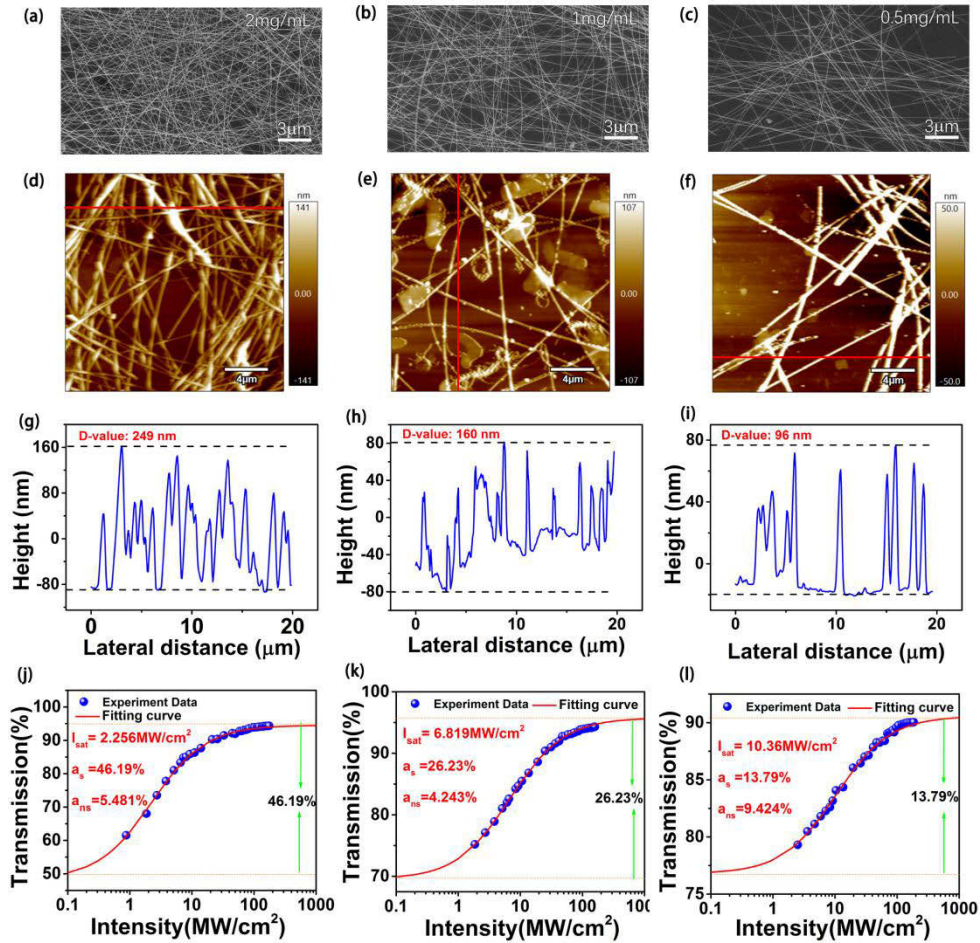


**Fig. 2.** The SEM, AFM and nonlinear transmission property of AgNW which with the concentrations of (a)(d)(g)(j) 2 mg/mL, (b)(e)(h)(k) 1 mg/mL and (c)(f)(i)(l) 0.5 mg/mL.

### 3. Experiment

As depicted in Fig. 3, the optical nonlinearity of AgNW SA is explored using a classical ring cavity fiber laser. The whole system operates in the state of anomalous dispersion of  $-0.032 \text{ ps}^2$  with a total length of 2.7 m. The length of erbium-doped fiber (EDF, Liekki 110-4/125) used is measured as 0.4 m. By a wavelength-division multiplexer (976/1550 WDM), the pump light from a 976 nm laser diode is coupled into the cavity. Using a 20:80 optical coupler (OC), 20% of laser power is exported to accomplish further detection and observation. The isolator (ISO) guarantees the unidirectional laser operation, which protects the related optical devices in the cavity and enhances the efficiency of operation. The evolution of laser polarization state in the cavity can be regulated within a certain range by using a polarization controller (PC). An oscilloscope is used to monitor the transmission status of intra-cavity pulses and record the pulse information in real time. An optical spectrum analyzer and radio frequency (RF) spectrum analyzer are used to collect relevant subsequent supplementary data.

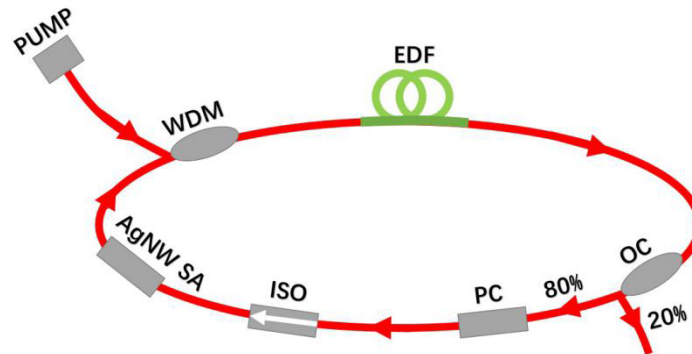


Fig. 3. Schematic diagram of AgNW-based QSFL.

#### 4. Results and discussion

For comparison experiments, three samples with different concentrations are prepared and applied to the experiment in turn. Firstly, sample 1 is coupled into the ring cavity, and the stable Q-switched sequences are observed for the first time when the pump power increased to 167 mW. The performance of QSFL based on sample 1 is summarized in Fig. 4. From the evolution of the output pulse sequences in Fig. 4(a), the repetition rate of pulses increases and the pulses in finite time become more and more intensive at high power. In Fig. 4(b), the pulse duration of achieved Q-switched pulses is 838.4 ns when the pump power is 630 mW (maximum value). From Fig. 4(c), the operating wavelength of the Q-switched system is located at 1559.88 nm, the 3-dB spectral bandwidth is 1.53 nm. The monitoring of the spectrum for up to 15 hours demonstrates the high pulse quality and stability of the system. The resolution of the optical spectrum is 2 nm. The radio frequency (RF) spectrum about fundamental frequency and frequency multiplication (illustration) are revealed in Fig. 4(d). The signal-to-noise ratio (SNR) is given as 55.7 dB at a resolution of 30 Hz. The large SNR and the uniform trend of frequency multiplication indicate the stability of the system. The trends of power-dependent repetition rate and pulse duration are revealed in Fig. 4(e). From Fig. 4(f), the maximum output power is given as 32.9 mW. Correspondingly, the pulse energy is calculated as 139 nJ.

Subsequently, sample 2 replaced sample 1 in the same way where the experimental environment remains unchanged. The Q-switching threshold of the system is 212 mW. Similar to sample 1, the main information of the Q-switched pulse is summarized in Fig. 5, which shows that the pulse duration of QSFL employing sample 2 is 536 ns. The SNR of fundamental frequency Fig. 5(b) is 53 dB. The evolution process of power-dependent pulse duration and repetition rate are described in Fig. 5(c). Similarly, the maximum output power and pulse energy of QSFL employing sample 2 are given in Fig. 5(d), which are 34.7 mW and 142 nJ, respectively.

Finally, sample 3 is applied in the cavity in the same way. When the pump power increases to 276 mW, a stable Q-switched pulse sequence appears as shown in Fig. 6. The pulse duration in Fig. 6(a) is measured as 764 ns. The SNR is up to 50 dB as shown in Fig. 6(b). The maximum output power is 30.2 mW as shown in Fig. 6(d). The optical damage threshold of samples 1, 2 and 3 are 218.6 mJ/cm<sup>2</sup>, 223.3 mJ/cm<sup>2</sup>, and 199.7 mJ/cm<sup>2</sup>, respectively. To discover the performance differences between the three lasers more intuitively, the main data are summarized in Table 1.

During the experiment, the three SAs have environmental stability. The comparison of the data in Table 1 indicates that the Q-switching threshold of the laser based on sample 1 is the smallest, which may be related to the saturation intensity of samples. When the spontaneous emission in the cavity is greater than the saturation intensity of absorption, the absorption coefficient of SA decreases, resulting in laser oscillation and Q-switched pulse output. Therefore, a smaller

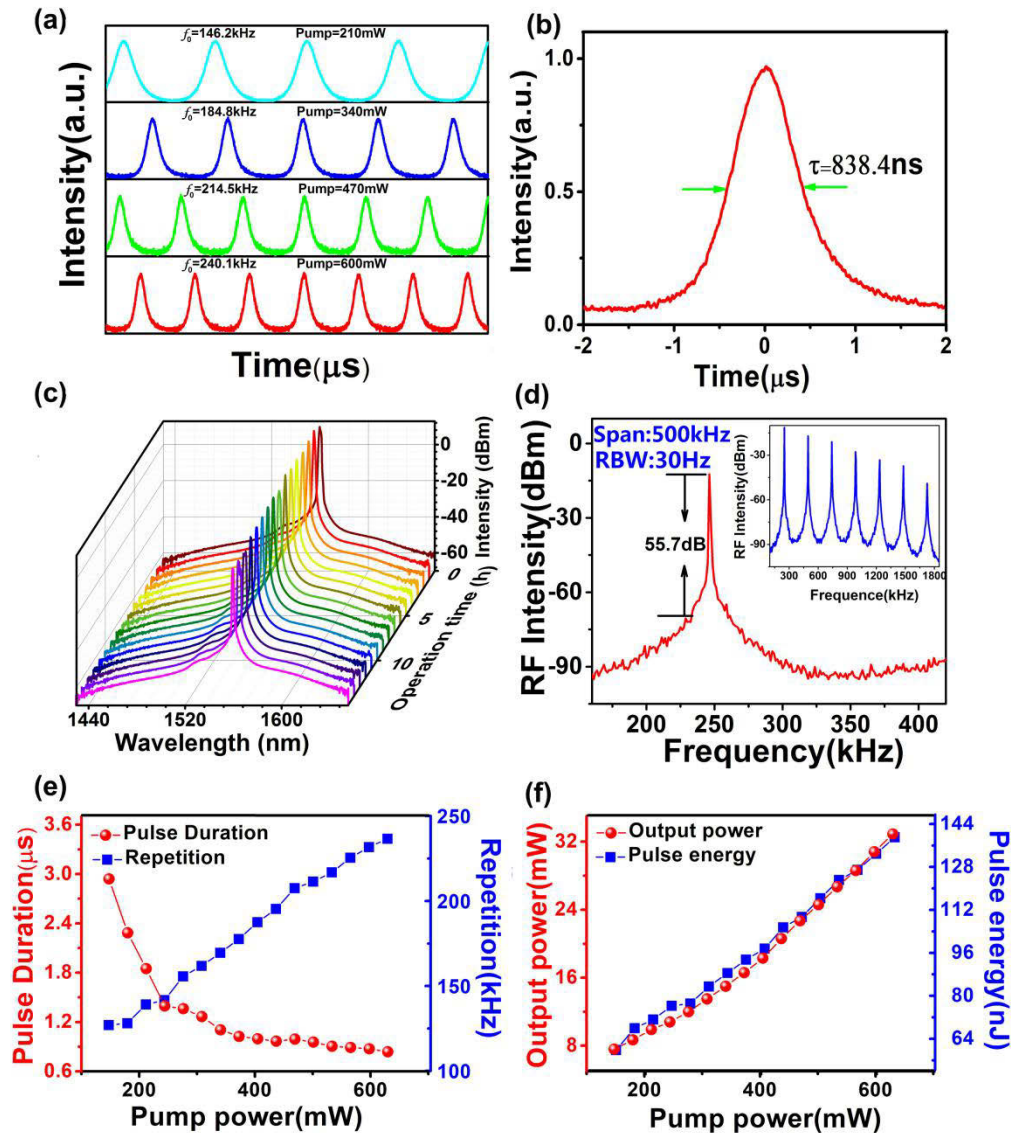


**Fig. 4.** Performance of QSFL based on sample 1. (a) Evolution of the output pulse sequence; (b) Pulse duration; (c) Spectrum; (d) RF spectrum; (e) The power-dependent functions of repetition rate and pulse duration; (f) The power-dependent functions of pulse energy and output power.

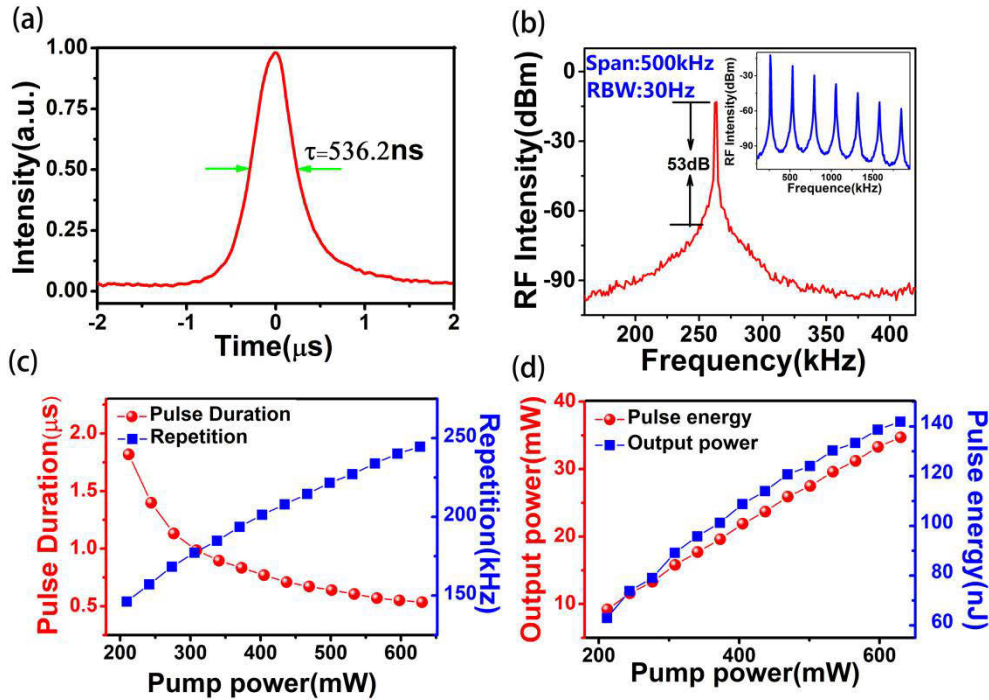


**Fig. 5.** Performance of QSFL based on sample 2. (a) Pulse duration; (b) RF spectrum; (c) Trends of power-dependent repetition rate and pulse duration; (d) Trends of power-dependent output power and pulse energy.

**Table 1.** Performance of QSFLs based on three samples.

Material	MD(%) $I_{\text{sat}}$ (MW/cm <sup>2</sup> )	Threshold (mW)	RF (kHz)	$\lambda_c$ (nm)	$\tau$ ( $\mu$ s)	SNR (dB)	IL (dB)	P (mW)	Pulse energy (nJ)
Sample 1 (2mg/mL)	46.19/2.256	167	127-236.6	1559.8	0.838-2.94	55.7	0.25	32.9	139
Sample 2 (1mg/mL)	26.23/6.819	212	146.2-244.5	1559.8	0.536-1.818	53	0.19	34.7	142
Sample 3 (0.5mg/mL)	13.79/10.36	276	164.5-237	1557.4	0.764-2.516	50	0.43	30.2	127

saturation intensity is beneficial to the generation of Q-switched sequences. The value of the modulation depth affects the stability of the system. When the modulation depth is larger, the stability of the system is better, which is consistent with previous research [46]. Besides, we note that the output power of laser based on the device with larger insertion loss (IL) is smaller. As for the pulse duration of laser, this may be the result of the combined action of modulation depth, saturation intensity, and unsaturated loss, etc. We can not assert which of these factors is more effective, as the detailed mechanism of these parameters is still unknown to us, but we believe that there is an optimal concentration in achieving the shortest pulses.

As shown in Table 2, the performances of various similar QSFLs are enumerated. From the aspect of pulse duration, the pulse duration as low as 536 ns is competitive from Table 2, which illustrates the potential of AgNW for the generation of ultrashort pulses. Furthermore, the average output power is also an important indicator for evaluating the performance of the laser.

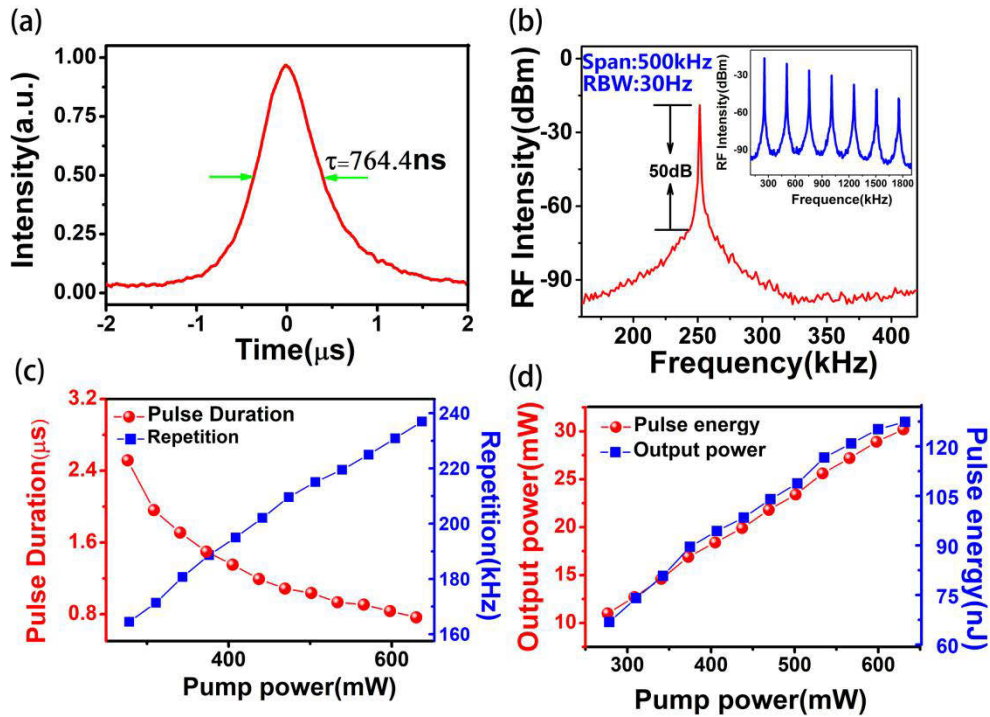


**Fig. 6.** Performance of QSFL based on sample 3. (a) Pulse duration; (b) RF spectrum; (c) Trends of power-dependent repetition rate and pulse duration; (d) Trends of power-dependent output power and pulse energy.

Considering the wide application of Q-switched lasers in laser processing, the demand for high power is inevitable and important. In general, the average output powers of SA-based lasers are less than 25 mW. However, the power of the implemented laser is up to 34.7 mW, which indicates the great prospect of AgNW in the realization of a high power laser.

**Table 2.** Performance comparisons of SA- based QSFLs

Material	Repetition frequency (kHz)	$\tau$ ( $\mu$ s)	SNR (dB)	Output power (mW)	Pulse energy (nJ)	Ref.
Bi <sub>2</sub> Se <sub>3</sub>	495-940	1.9-7.79	50	22.35	23.7	[47]
MoS <sub>2</sub>	8.77-43.47	3.3-26.7	50	5.91	160	[48]
WS <sub>2</sub>	82-134	0.71	25	2.5	19	[49]
BP	5.73-31.07	25.77-63.59	46	4	142.6	[50]
MoSe <sub>2</sub>	66.847	6.506	31.3	2.45	369.5	[51]
Gold nanorods	7.1-39.9	4.8-23	-	12.5	-	[52]
AgNW(1mg/mL)	146.2-244.5	0.536-1.818	53	34.7	142	This work

## 5. Conclusion

In the experiment, the nonlinear optical properties of proposed AgNW SAs have been investigated in QSFLs. Meanwhile, the effects of three different AgNW SAs on QSFLs have been explored through comparative experiments. Comparing the performance of three different QSFLs, it is

found that the concentration, saturation intensity, insertion loss and modulation depth of AgNW SA have a great influence on the performance of QSFLs. Moreover, compared with previously reported QSFLs, AgNW-based lasers have great potential in the generation of ultrashort pulses. This is not only the first successful attempt of AgNW in QSFLs, but also provides a meaningful reference for further research on the application of AgNW, paving the way for the engineering design of related optical devices.

## Funding

National Natural Science Foundation of China (11674036, 11875008, 91850209); Beijing Youth Top-Notch Talent Support Program (2017000026833ZK08); Fund of State Key Laboratory of Information Photonics and Optical Communications, Beijing University of Posts and Telecommunications (IPOC2019ZZ01); Fundamental Research Funds for the Central Universities (500419305); State Key Laboratory of Advanced Optical Communication Systems and Networks, Shanghai Jiao Tong University (2019GZKF03007); Beijing University of Posts and Telecommunications Excellent Ph.D. Students Foundation (CX2019202).

## Disclosures

The authors declare that there are no conflicts of interest related to this article.

## References

1. R. Valiev, "Materials science: nanomaterial advantage," *Nature* **419**(6910), 887–889 (2002).
2. K. S. Novoselov, A. K. Geim, S. V. Morozov, D. Jiang, Y. Zhang, S. V. Dubonos, I. V. Grigorieva, and A. A. Firsov, "Electric field effect in atomically thin carbon films," *Science* **306**(5696), 666–669 (2004).
3. A. C. Ferrari, J. C. Meyer, V. Scardaci, C. Casiraghi, M. Lazzeri, F. Mauri, S. Piscanec, D. Jiang, K. S. Novoselov, S. Roth, and A. K. Geim, "Raman spectrum of graphene and graphene layers," *Phys. Rev. Lett.* **97**(18), 187401 (2006).
4. S. Stankovich, D. A. Dikin, G. H. B. Dommett, K. M. Kohlhaas, E. J. Zimney, E. A. Stach, R. D. Piner, S. T. Nguyen, and R. S. Ruoff, "Graphene-based composite materials," *Nature* **442**(7100), 282–286 (2006).
5. A. K. Geim and K. S. Novoselov, "The rise of graphene," *Nat. Mater.* **6**(3), 183–191 (2007).
6. Q. Bao, H. Zhang, Y. Wang, Z. Ni, Y. Yan, Z. Shen, K. P. Loh, and D. Tang, "Atomic-layer graphene as a saturable absorber for ultrafast pulsed lasers," *Adv. Funct. Mater.* **19**(19), 3077–3083 (2009).
7. Z. Sun, T. Hasan, F. Torrisi, D. Popa, G. Privitera, F. Wang, F. Bonaccorso, D. M. Basko, and A. C. Ferrari, "Graphene mode-locked ultrafast laser," *ACS Nano* **4**(2), 803–810 (2010).
8. M. Xu, T. Liang, M. Shi, and H. Chen, "Graphene-like two-dimensional materials," *Chem. Rev.* **113**(5), 3766–3798 (2013).
9. G. Fiori, F. Bonaccorso, G. Iannaccone, T. Palacios, D. Neumaier, A. Seabaugh, S. K. Banerjee, and L. Colombo, "Electronics based on two-dimensional materials," *Nat. Nanotechnol.* **9**(10), 768–779 (2014).
10. S. Z. Butler, S. M. Hollen, L. Cao, Y. Cui, J. A. Gupta, H. R. Gutiérrez, T. F. Heinz, S. Sae Hong, J. Huang, A. F. Ismach, E. Johnston-Halperin, M. Kuno, V. V. Plashnitsa, R. D. Robinson, R. S. Ruoff, S. Salahuddin, J. Shan, L. Shi, M. G. Spencer, M. Terrones, W. Windl, and J. E. Goldberger, "Progress, challenges, and opportunities in two-dimensional materials beyond graphene," *ACS Nano* **7**(4), 2898–2926 (2013).
11. W. Liu, L. Pang, H. Han, W. Tian, H. Chen, M. Lei, P. Yan, and Z. Wei, "70-fs mode-locked erbium-doped fiber laser with topological insulator," *Sci. Rep.* **6**(1), 19997 (2016).
12. P. Yan, R. Lin, S. Ruan, A. Liu, and H. Chen, "A 2.95 GHz, femtosecond passive harmonic mode-locked fiber laser based on evanescent field interaction with topological insulator film," *Opt. Express* **23**(1), 154–164 (2015).
13. H. Zhang, S. Lu, J. Zheng, J. Du, S. Wen, D. Tang, and K. P. Loh, "Molybdenum disulfide (MoS<sub>2</sub>) as a broadband saturable absorber for ultra-fast photonics," *Opt. Express* **22**(6), 7249–7260 (2014).
14. K. Wu, B. Chen, X. Zhang, S. Zhang, C. Guo, C. Li, P. Xiao, J. Wang, L. Zhou, W. Zou, and J. Chen, "High-performance mode-locked and Q-switched fiber lasers based on novel 2D materials of topological insulators, transition metal dichalcogenides and black phosphorus: review and perspective," *Opt. Commun.* **406**, 214–229 (2018).
15. H. Tang, J. Wang, H. Yin, H. Zhao, D. Wang, and Z. Tang, "Growth of polypyrrole ultrathin films on MoS<sub>2</sub> monolayers as high-performance supercapacitor electrodes," *Adv. Mater.* **27**(6), 1117–1123 (2015).
16. M. Dahbi, N. Yabuuchi, M. Fukunishi, K. Kubota, K. Chihara, K. Tokiwa, X. Yu, H. Ushiyama, K. Yamashita, J. Son, Y. Cui, H. Oji, and S. Komaba, "Black phosphorus as a high-capacity, high-capability negative electrode for sodium-ion batteries: investigation of the electrode/electrolyte interface," *Chem. Mater.* **28**(6), 1625–1635 (2016).
17. H. Peng, W. Dang, J. Cao, Y. Chen, D. Wu, W. Zheng, H. Li, Z. Shen, and Z. Liu, "Topological insulator nanostructures for near-infrared transparent flexible electrodes," *Nat. Chem.* **4**(4), 281–286 (2012).

18. P. Yasaei, A. Behranginia, T. Foroozan, M. Asadi, K. Kim, F. Khalili-Araghi, and A. Salehi-Khojin, "Stable and selective humidity sensing using stacked black phosphorus flakes," *ACS Nano* **9**(10), 9898–9905 (2015).
19. D. J. Late, Y. Huang, B. Liu, J. Acharya, S. N. Shirodkar, J. Luo, A. Yan, D. Charles, U. V. Waghmare, V. P. Dravid, and C. N. R. Rao, "Sensing behavior of atomically thin-layered MoS<sub>2</sub> transistors," *ACS Nano* **7**(6), 4879–4891 (2013).
20. K. K. Liu, W. Zhang, Y. H. Lee, Y. C. Lin, M. T. Chang, C. Y. Su, C. S. Chang, H. Li, Y. Shi, H. Zhang, C. S. Lai, and L. J. Li, "Growth of large-area and highly crystalline MoS<sub>2</sub> thin layers on insulating substrates," *Nano Lett.* **12**(3), 1538–1544 (2012).
21. S. Lijima, "Helical microtubules of graphitic carbon," *Nature* **354**(6348), 56–58 (1991).
22. J. Hu, T. W. Odom, and C. M. Lieber, "Chemistry and physics in one dimension: Synthesis and properties of nanowires and nanotubes," *Acc. Chem. Res.* **32**(5), 435–445 (1999).
23. Z. Pan, Z. Dai, and Z. Wang, "Nanobelts of semiconducting oxides," *Science* **291**(5510), 1947–1949 (2001).
24. A. Pierret, M. Hocevar, S. L. Diedenhofen, R. E. Algra, E. Vlieg, E. C. Timmering, M. A. Verschuuren, G. W. G. Immink, M. A. Verheijen, and E. P. A. M. Bakkers, "Generic nano-imprint process for fabrication of nanowire arrays," *Nanotechnology* **21**(6), 065305 (2010).
25. H. Liang, S. Liu, and S. Yu, "Controlled synthesis of one-dimensional inorganic nanostructures using pre-existing one-dimensional nanostructures as templates," *Adv. Mater.* **22**(35), 3925–3937 (2010).
26. Z. Li, F. Hao, Y. Huang, Y. Fang, P. Nordlander, and H. Xu, "Directional light emission from propagating surface plasmons of silver nanowires," *Nano Lett.* **9**(12), 4383–4386 (2009).
27. W. J. Liu, M. L. Liu, S. Lin, J. C. Liu, M. Lei, H. Wu, C. Q. Dai, and Z. Y. Wei, "Synthesis of high quality silver nanowires and their applications in ultrafast photonics," *Opt. Express* **27**(12), 16440–16448 (2019).
28. S. Lin, J. C. Liu, W. Z. Li, D. Wang, Y. Huang, C. Jia, Z. W. Li, H. Y. Wang, J. N. Song, Z. L. Liu, K. Huang, D. Zu, M. Lei, B. Hong, and H. Wu, "A Flexible, Robust and Gel-Free Electroencephalogram Electrode for Noninvasive Brain-Computer Interfaces," *Nano Lett.* **19**(10), 6853–6861 (2019).
29. S. Lin, X. P. Bai, H. Y. Wang, H. L. Wang, J. N. Song, K. Huang, C. Wang, N. Wang, B. Li, M. Lei, and H. Wu, "Roll-to-Roll Production of Transparent Silver Nanofiber Network Electrode for Flexible Electrochromic Smart Windows," *Adv. Mater.* **29**(41), 1703238 (2017).
30. S. Lin, H. Y. Wang, X. N. Zhang, D. Wang, D. Zu, J. N. Song, Z. L. Liu, Y. Huang, K. Huang, N. Tao, Z. W. Li, X. P. Bai, B. Li, M. Lei, Z. F. Yu, and H. Wu, "Direct Spray-Coating of Highly Robust and Transparent Ag Nanowires for Energy Saving Windows," *Nano Energy* **62**, 111–116 (2019).
31. S. Lin, H. Y. Wang, F. Wu, Q. M. Wang, X. P. Bai, D. Zu, J. N. Song, D. Wang, Z. L. Liu, Z. W. Li, N. Tao, K. Huang, M. Lei, B. Li, and H. Wu, "Room-temperature production of silver-nanofiber film for large-area, transparent and flexible surface electromagnetic interference shielding," *npj Flexible Electron.* **3**(1), 6 (2019).
32. J. Zou, Z. Kang, R. Wang, H. Wang, J. Liu, C. Dong, X. Jiang, B. Xu, Z. Cai, G. Qin, H. Zhang, and Z. Luo, "Green/red pulsed vortex-beam oscillations in all-fiber lasers with visible-resonance gold nanorods," *Nanoscale* **11**(34), 15991–16000 (2019).
33. Q. Du, Z. Luo, H. Zhong, Y. Zhang, Y. Huang, T. Du, W. Zhang, T. Gu, and J. Hu, "Chip-scale broadband spectroscopic chemical sensing using an integrated supercontinuum source in a chalcogenide glass waveguide," *Photonics Res.* **6**(6), 506–510 (2018).
34. W. Li, J. Zou, Y. Huang, K. Wang, T. Du, S. Jiang, and Z. Luo, "212-kHz-linewidth, transform-limited pulses from a single-frequency Q-switched fiber laser based on a few-layer Bi<sub>2</sub>Se<sub>3</sub> saturable absorber," *Photonics Res.* **6**(10), C29–C35 (2018).
35. W. J. Kwak, H. G. Jung, S. H. Lee, J. B. Parka, D. Aurbach, and Y. K. Suna, "Silver nanowires as catalytic cathodes for stabilizing lithium-oxygen batteries," *J. Power Sources* **311**, 49–56 (2016).
36. L. Hu, H. S. Kim, J. Y. Lee, P. Peumans, and Y. Cui, "Scalable coating and properties of transparent, flexible, silver nanowire electrodes," *ACS Nano* **4**(5), 2955–2963 (2010).
37. S. Yao and Y. Zhu, "Wearable multifunctional sensors using printed stretchable conductors made of silver nanowires," *Nanoscale* **6**(4), 2345–2352 (2014).
38. S. H. Lee, S. Lim, and H. Kim, "Smooth-surface silver nanowire electrode with high conductivity and transparency on functional layer coated flexible film," *Thin Solid Films* **589**, 403–407 (2015).
39. A. Tao, F. Kim, C. Hess, J. Goldberger, R. He, Y. Sun, Y. Xia, and P. Yang, "Langmuir-Blodgett silver nanowire monolayers for molecular sensing using surface-enhanced Raman spectroscopy," *Nano Lett.* **3**(9), 1229–1233 (2003).
40. B. Thirumalraj, D. H. Zhao, S. M. Chen, and S. Palanisamy, "Non-enzymatic amperometric detection of hydrogen peroxide in human blood serum samples using a modified silver nanowire electrode," *J. Colloid Interface Sci.* **470**, 117–122 (2016).
41. Y. P. Han, J. L. Sun, H. A. Ye, W. Z. Wu, and G. Shi, "Nonlinear refraction of silver nanowires from nanosecond to femtosecond laser excitation," *Appl. Phys. B* **94**(2), 233–237 (2009).
42. J. Wang, H. Chen, Z. Jiang, J. Yin, J. Wang, M. Zhang, T. He, J. Li, P. Yan, and S. Ruan, "Mode-locked thulium-doped fiber laser with chemical vapor deposited molybdenum ditelluride," *Opt. Lett.* **43**(9), 1998–2001 (2018).
43. Q. Ding, Y. Shi, M. Chen, H. Li, X. Yang, Y. Qu, W. Liang, and M. Sun, "Ultrafast dynamics of plasmon-exciton interaction of Ag nanowire-graphene hybrids for surface catalytic reactions," *Sci. Rep.* **6**(1), 32724 (2016).
44. Q. Bao, H. Zhang, Z. Ni, Y. Wang, L. Polavarapu, Z. Shen, Q. Xu, D. Tang, and K. Loh, "Monolayer graphene as a saturable absorber in a mode-locked laser," *Nano Res.* **4**(3), 297–307 (2011).

45. V. G. Pol, D. N. Srivastava, O. Palchik, V. Palchik, M. A. Slifkin, A. M. Weiss, and A. Gedanken, "Sonochemical deposition of silver nanoparticles on silica spheres," *Langmuir* **18**(8), 3352–3357 (2002).
46. R. Wei, H. Zhang, X. Tian, T. Qiao, Z. Hu, Z. Chen, X. He, Y. Yua, and J. Qiu, "MoS<sub>2</sub> nanoflowers as high performance saturable absorbers for an all-fiber passively Q-switched erbium-doped fiber laser," *Nanoscale* **8**(14), 7704–7710 (2016).
47. Z. Yu, Y. Song, J. Tian, Z. Dou, H. Guoyu, K. Li, H. Li, and X. Zhang, "High-repetitionrate Q-switched fiber laser with high quality topological insulator Bi<sub>2</sub>Se<sub>3</sub> film," *Opt. Express* **22**(10), 11508–11515 (2014).
48. Y. Huang, Z. Luo, Y. Li, M. Zhong, B. Xu, K. Che, H. Xu, Z. Cai, J. Peng, and J. Weng, "Widely-tunable, passively Q-switched erbium-doped fiber laser with few-layer MoS<sub>2</sub> saturable absorber," *Opt. Express* **22**(21), 25258–25266 (2014).
49. S. H. Kassani, R. Khazaeinezhad, H. Jeong, T. Nazari, D. I. Yeom, and K. Oh, "All-fiber Er-doped Q-switched laser based on tungsten disulfide saturable absorber," *Opt. Mater. Express* **5**(2), 373–379 (2015).
50. T. Feng, D. Mao, X. Cui, M. Li, K. Song, B. Jiang, H. Lu, and W. Quan, "A Filmy blackphosphorus polyimide saturable absorber for Q-switched operation in an erbium-doped fiber laser," *Materials* **9**(11), 917 (2016).
51. B. Chen, X. Zhang, K. Wu, H. Wang, J. Wang, and J. Chen, "Q-switched fiber laser based on transition metal dichalcogenides MoS<sub>2</sub>, MoSe<sub>2</sub>, WS<sub>2</sub>, and WSe<sub>2</sub>," *Opt. Express* **23**(20), 26723–26737 (2015).
52. Z. Kang, X. Guo, Z. Jia, Y. Xu, L. Liu, D. Zhao, G. Qin, and W. Qin, "Gold nanorods as saturable absorbers for all-fiber passively Q-switched erbium-doped fiber laser," *Opt. Mater. Express* **3**(11), 1986–1991 (2013).